ACES Asian Chemical Editorial Society

VIP

Special Collection

A Low-Temperature Molecular Precursor Approach to Copper-Based Nano-Sized *Digenite* Mineral for Efficient Electrocatalytic Oxygen Evolution Reaction

Biswarup Chakraborty+,[a] Shweta Kalra+,[a] Rodrigo Beltrán-Suito,[a] Chittaranjan Das,[b] Tim Hellmann,[c] Prashanth W. Menezes,*[a] and Matthias Driess*[a]

Abstract: In the urge of designing noble metal-free and sustainable electrocatalysts for oxygen evolution reaction (OER), herein, a mineral *Digenite* Cu_9S_5 has been prepared from a molecular copper(I) precursor, $[\{(PyHS)_2Cu^I(PyHS)\}_2]$ $(OTf)_2$ (**1**), and utilized as an anode material in electrocatalytic OER for the first time. A hot injection of **1** yielded a pure phase and highly crystalline Cu_9S_5, which was then electrophoretically deposited (EPD) on a highly conducting nickel foam (NF) substrate. When assessed as an electrode for OER, the Cu_9S_5/NF displayed an overpotential of merely 298 ± 3 mV at a current density of 10 mA cm^{-2} in alkaline media. The overpotential recorded here supersedes the value obtained for the best reported Cu-based as well as the benchmark precious-metal-based RuO_2 and IrO_2 electrocatalysts. In addition, the choronoamperometric OER indicated the superior stability of Cu_9S_5/NF, rendering its suitability as the sustainable anode material for practical feasibility. The excellent catalytic activity of Cu_9S_5 can be attributed to the formation of a crystalline CuO overlayer on the conductive Cu_9S_5 that behaves as active species to facilitate OER. This study delivers a distinct molecular precursor approach to produce highly active copper-based catalysts that could be used as an efficient and durable OER electro(pre)catalysts relying on non-precious metals.

Introduction

Increasing consumption of fossil fuels by mankind leads to a fast depletion of natural abundant fuels and therefore, an urgent requirement of alternative resources to harvest energy has become a global issue.[1] Spitting of water into oxygen (O_2) and subsequent production of hydrogen (H_2), an alternative non-carbonaceous fuel, is one of the promising approaches to store renewable electricity.[2] However, oxidation of water to oxygen or OER is the most fascinating reaction occurs in natural photosynthesis harvesting photon to convert solar energy to chemical energy.[3] Although, by mimicking nature's strategy, artificial photosynthesis scheme has become a promising approach for clean and sustainable energy production,[4] the large thermodynamic barrier of the OER, and the complicated reaction kinetics make this process potentially challenging.[5] Thus, the design of an efficient catalyst for OER remains a perdurable challenge and requires immense attention.[6] Currently, the oxides of Ir or Ru have been considered to be the state-of-the-art electrocatalysts for OER, however, the exorbitant cost and scarcity of these noble metals seriously limit their large-scale practical applications.[7] A large number of transition metal-based materials such as oxides,[8] chalcogenides,[9] pnictides,[10] intermetallics,[11] phosphates,[12] phosphites[13] and borophosphates[12,14] have been regarded as attractive electrocatalysts for the OER and the further improvement of electrocatalytic activity and durability through synthesis and design methods is still a great challenge.[12–14,15]

Despite the low cost, environmentally benign, a high electrical conductivity[16] and promising catalytic activity,[17] of copper-based materials, only in a handful of cases, copper-chalcogenides have been used for electrocatalytic OER study.[17c,18] In this direction, Cu_2S nanostructure was found to be the best pure Cu-based anode material with considerably good OER activity with a low overpotential of 336 mV (at 10 mA cm^{-2}).[18a] A recent study has suggested that the efficiency of CuS for OER could be enhanced by the incorporation of second transition metal ion into the structure.[19] Similarly, some of the copper-chalcogenides ($Cu_{2-x}Se$) -pnictides

[a] Dr. B. Chakraborty,+ S. Kalra,+ R. Beltrán-Suito, Dr. P. W. Menezes, Prof. Dr. M. Driess
Department of Chemistry
Metalorganics and Inorganic Materials
Technische Universität Berlin
Straße des 17 Juni 135, Sekr. C2, 10623 Berlin (Germany)
E-mail: prashanth.menezes@mailbox.tu-berlin.de
matthias.driess@tu-berlin.de

[b] Dr. C. Das
Karlsruhe Institute of Technology (KIT)
Institute for Applied Materials (IAM-ESS)
Hermann-von-Helmholtz-Platz 1, D-76344 Eggenstein-Leopoldshafen (Germany)

[c] T. Hellmann
Surface Science Division
Department of Materials Science
Technical University Darmstadt
Otto-Berndt-Str. 3, 64287 Darmstadt (Germany)

[+] Authors contributed equally

(Cu_3N, Cu_3P) and -oxides have also shown promising catalytic OER activity along with long-term durability.[10c, 20]

Within the various synthetic methods applied for the design of OER electrocatalysts, the low-temperature molecular precursor approach has recently shown enormous advantages such as better atomic-level control over the stoichiometry, uniformly distributed nano-sized particles, homogenous elemental dispersion, and unique electronic and surface structure, over traditional high-temperature techniques.[21] Taking advantage of this approach, we recently demonstrated excellent electro-catalytic water splitting performance of molecularly derived $FeSe_2$, FeP, CoP and $NiPt_3@NiS$ nanostructures starting from a molecular complex supported by organic nitrogen donor ligands.[9,10a,b,22] In this context, 2-mercaptopyridine, an organo-sulfur compound, existing as an equilibrium of tautomeric mixture of 2-pyridine-thiol (PySH) and 2-pyridine-thione (PyHS),[23] including a zwitterionic structure (PyH^+S^-)[24] (Scheme 1, square box) has been utilized as versatile sulfur donor ligand to isolate diverse transition metal complexes and could be an attractive choice to produce metal sulfide nanostructures.[25]

In this work, we report a simple single-step synthetic protocol to the homodinuclear copper(I) complex, $[\{(PyHS)_2Cu^I(PyHS)\}_2](OTf)_2$ (1) with a square-planar $\{Cu^I_2S_2\}$ core. Each copper center in **1** adopts a distorted tetrahedral geometry surrounded by four 2-pyridine-SH ligands and both copper centers are connected via two bridging μ_2-S donor atoms of two terminal 2-pyridine-thione (PyHS) units. The $\{Cu^I_2S_2\}$ core complex has been utilized as an suitable low-temperature molecular precursor to isolate the highly crystalline mineral *Digenite* Cu_9S_5 as an efficient OER electro(pre)catalyst in an alkaline electrolyte. The Cu_9S_5 nanostructures acquired through the hot-injection of **1** have been deposited on highly conducting NF electrode substrate through the EPD technique without affecting the chemical identity. The fabricated Cu_9S_5/NF electrocatalyst requires an overpotential of only 298 ± 3 mV to attain a current density of $10 \, mA \, cm^{-2}$, outperforming benchmark copper-based and even noble metal-based OER catalysts. Apart from low overpotential, the Cu_9S_5/NF has also been demonstrated to be a stable catalyst on a longer run. Post-OER analyses indicated the formation of crystalline CuO overlayer on Cu_9S_5, which acts as an active phase for OER while the conductive inner core accelerates the electron mobility. The presented study shows a promising scope to explore new defined transition metal-based molecular structures to derive the unexplored class of functional materials for electrocatalytic applications beyond water splitting.

Results and Discussion

The molecular precursor complex, $[\{(PyHS)_2Cu^I(PyHS)\}_2](OTf)_2$ (**1**), was isolated as crystalline yellow powder from a mixture of copper(II) triflate and 2-mercaptopyridine (with a molar ratio of 1:4) in dichloromethane (Scheme 1). The purity of the isolated complex was verified by elemental analysis, which precisely matched with the calculated values. The Fourier-transform infrared spectrum (FT-IR) of the isolated complex depicts two strong vibrations at 1127 and 1366 cm^{-1} attributed to the vibrations of $\nu(S=O)$ and $\nu(C-F)$, respectively, of the triflate counter anion (Figure S1). The electrospray ionization (ESI) mass spectrum of **1** (in tetrahydrofuran, positive ion mode) exhibited major molecular ion peaks at m/z value of 284.96, 361.98 and 395.97 with an expected isotopic distribution calculated for the molecular fragments, $[\{(PyHS)_2Cu\}]^+$, $[\{(PyHS)(PyS)Cu(Py)\}]^+$ and $[(PyHS)_3Cu]^+$, respectively (Figure S2). The ^1H NMR spectrum of **1** in CD_3CN revealed resonances of the aromatic protons at the chemically indistinguishable pyridine ring of the 2-mercapto-thiol ligand within the range of 7 to 12.5 ppm, which unambiguously confirms the diamagnetic nature of the complex (Figure S3). Moreover, the high-resolution Cu 2p X-ray photoelectron (XPS) spectra obtained with **1** further confirmed the presence of Cu^I while the valances of S 2p, N 1s, O 1s, and C 1s are also consistent with the structure determined from the as-synthesized crystalline powders (Figure S4). Although a copper(I) complex, similar to **1**, has been isolated previously from a reaction mixture of copper(II) halide and 2-mercaptopyridine,[26] the redox non-innocent behavior of 2-mercaptopyridine, in-situ reduction of iron(III) to an isolable mononuclear iron(II) complex, $[Fe^{II}(PySH)_4](ClO_4)_2$, was reported only recently.[25b]

Single-crystals grown from a concentrated acetonitrile solution of **1** belong to a monoclinic space group *I*2/*m* (Table S1). X-ray structure determination confirmed the presence of two triflate counter ions along with a dinuclear copper-sulphur cluster as dicationic entity, very similar to [Cu^I
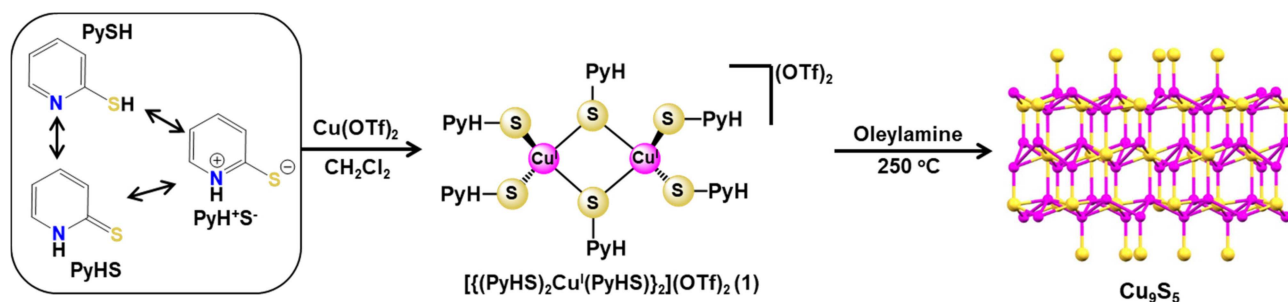
Scheme 1. Synthesis of the dinuclear copper(I) complex **1**, $[\{(PyHS)_2Cu^I(PyS)_2\}](OTf)_2$, using the 2-mercaptopyridine as supporting ligand. The square planar $\{Cu^I_2S_2\}$ core in **1** was used as a single-source precursor to prepare the crystalline Cu_9S_5 nanostructure of the *Digenite* mineral (right; Cu: purple; S: yellow).

$(C_5H_5NS)_3]_2X_2$ (X=Cl, Br, $NO_3)^{[26b,c]}$ and $[Cu^I_2(dmpymtH)_6]_2$ (dmpymtH=4,6-dimethylpyrimidine-2-thione).[26a] The dication consists of an almost square-planar $\{Cu^I_2S_2\}$ core where the copper centers are distorted tetrahedral coordinated by two terminal monodentate PyHS and two μ_2-S-bridging PyHS ligands (Figure 1). The Cu-S distances and S—Cu—S angles are in the range of 2.293(1)-2.496(1) Å and 97.79(4)°−123.42(5)°, respectively, which are in good agreement with metric values of previously reported related transition-metal sulfides (Table S2).[25,26]

Using the single-source precursor approach, a crystalline black powder was isolated via hot-injection of **1** at 250 °C in
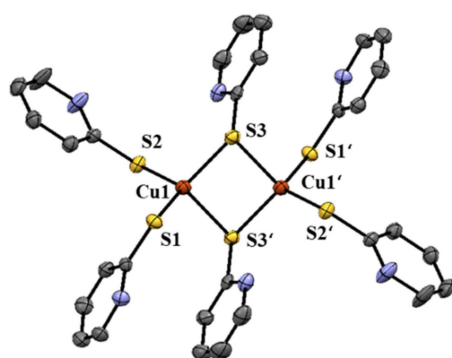

Figure 1. Molecular structure of the dication of **1**; thermal ellipsoid plot (40% probability). Colour code; carbon: grey, nitrogen: blue, sulphur: yellow, copper: red. All the hydrogen atoms of the protonated pyridine rings were omitted for clarity. The dicationic unit of **1** is symmetry generated from the half of its complete structure with a symmetry (') −x+3/2, −y+1/2, −z+1/2.

oleylamine (see Experimental Section).[9,10a,b,21,22] The crystalline structure, composition and phase purity of the as-obtained crystals of the particles was determined by powder X-ray diffraction (PXRD) technique. The XRD analysis of the as-prepared sample confirmed its high crystallinity and the reflections obtained correspond to the pure mineral *Digenite* Cu_9S_5 (JCPDS 47–1748) phase (Figure 2a). The solid-state crystal structure of Cu_9S_5 belongs to a rhombohedral, *R-3m* with lattice parameters a=3.930(1) Å and c=48.14(3) Å, respectively.[27] In Cu_9S_5, the mixed-valence copper centers comprise three different coordination geometries varying from trigonal planar to near square pyramidal with Cu—S distance of 2.285–2.880 Å resulting in a three-dimensional network (Figure S5).[27] The information on the atomic structure of Cu_9S_5 was provided by the transmission electron microscopy (TEM), which contained hexagon-shaped particles (Figure 2b). The high-resolution TEM image clearly indicated the d(101) lattice fringes with an interplanar distance of 0.33 nm (Figure 2c), further confirming the purity of the Cu_9S_5 product.[28] Additionally, the selected area electron diffraction (SAED) pattern of the particles displayed well-defined diffraction rings corresponding to the miller indices (101) and (1010) planes of Cu_9S_5 (Figure 2c, inset). The morphological features of pristine Cu_9S_5 were investigated by scanning electron microscopy (SEM) that exhibited a well-defined morphology in the aggregated particles (Figure 2d) and the subsequent elemental mapping of the particles confirmed the homogeneous distribution of Cu and S (Figure 2e-2f). The chemical composition of the particles was also evaluated by energy-dispersive X-ray spectroscopy and inductively coupled plasma atomic emission spectroscopy (ICP-AES) analyses evi-
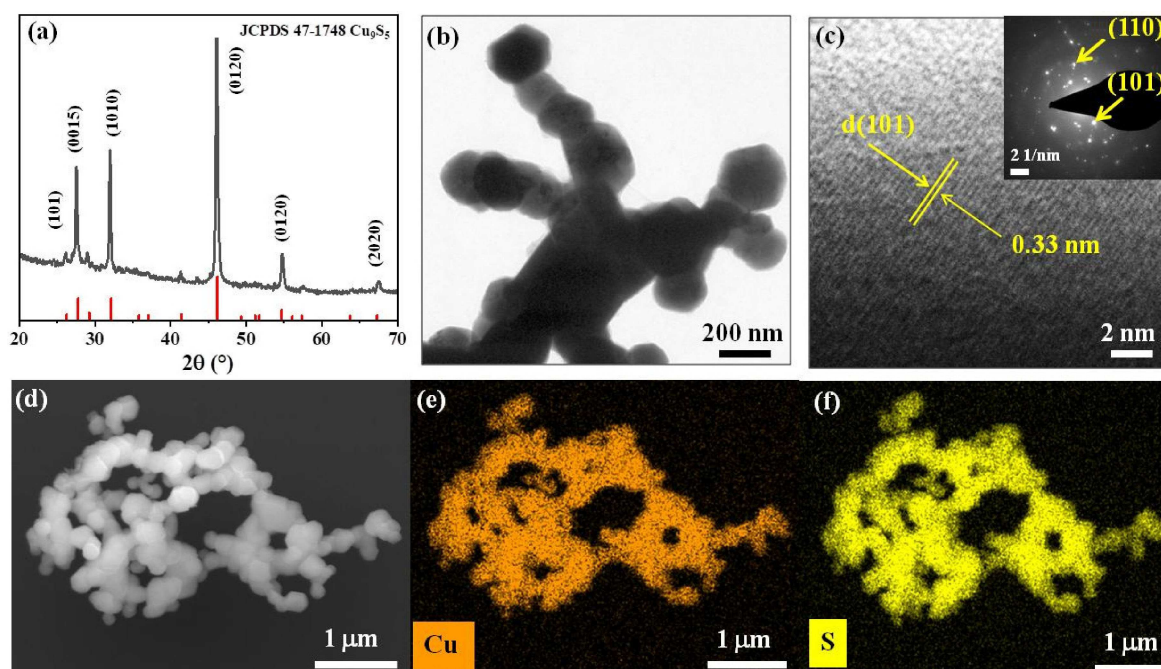

Figure 2. Structural characterization of as prepared CuS derived from molecular complex 1; (a) PXRD pattern displaying sharp reflections, corresponding to Cu_9S_5 (JCPDS-47-1748), (b) TEM images of Cu_9S_5 showing hexagonal-shaped nanocrystals (c) High-resolution TEM image with atomic fringes associated with the (101) lattice plane of Cu_9S_5, and SAED pattern exhibiting diffraction rings of Cu_9S_5 (inset), (d) SEM image of Cu_9S_5 particles with (e, f) EDX mapping revealing a homogenous distribution of elements Cu (orange) and S (yellow) (oxygen shown in Figure S6).

dencing the Cu:S ratio of ~1.80:1 (Figure S7, S8 and Table S3), which is consistent with the atomic composition of Cu_9S_5.

XPS analysis was utilized to study the surface electronic state and the composition of as-prepared Cu_9S_5. High-resolution core-level Cu 2p XPS spectrum displayed two major peaks at binding energy 932.1 and 952.2 eV, for $2p_{3/2}$ and $2p_{1/2}$, respectively. The binding energy values attained here clearly indicated the presence of Cu^I with minor amounts of Cu^{II}, which appeared due to surface oxidation of the materials and is common in non-oxidic Cu-based materials (Figure S9a).[19a,29] Furthermore, the spin-orbit coupling spacing value $(2p_{3/2}-2p_{1/2})$ of 19.6 eV also supported the Cu^I valency of copper in Cu_9S_5 (Figure S9a).[29] The S 2p spectrum showed the existence of doublet species with $2p_{3/2}$ binding energy located at 161.53 eV and the $2p_{1/2}$ binding energy at 163.8 eV, consistent with the presence of S^{II-} (Figure S9b).[29] The binding energies and the chemical composition attained by XPS analysis are in accordance with the earlier reports of Cu_9S_5 and Cu_2S materials.[17c,18a,b,d]

After a thorough microscopic and spectroscopic analysis, the Cu_9S_5 powder was deposited on NF through the EPD process.[11b,30] To ensure the chemical stability, the as-deposited Cu_9S_5 on NF were further analyzed by microscopic and analytical techniques, which demonstrated its unaltered stability upon EPD (Figure S10–S12). The OER activities of the as-synthesized Cu_9S_5/NF were investigated in a 1 M aqueous KOH electrolyte using a three-electrode cell. The polarization curve from the linear sweep voltammetry (LSV) displayed a continuous increment in current density up to 500 mA cm^{-2} at 1.7 V vs. RHE (Figure 3a), which clearly revealed catalytic oxidation of water. For comparison, CuO and Cu nanoparticles were also

synthesized, electrodeposited and measured in a similar condition. Remarkably, the overpotential of Cu_9S_5/NF electrode attained at 10 mA cm^{-2} was only 298±3 mV, which was lower than those of CuO/NF (340±4 mV), Cu/NF (390±3 mV), and bare NF electrode (490±5 mV). Incidentally, the electrocatalytic OER performance of Cu_9S_5/NF at higher current density (360± 4 mV at 100 mA cm^{-2}) was even better than CuO/NF (440± 4 mV), Cu/NF (550±3 mV), and noble metal-based RuO_2/NF (421±5 mV at 100 mA cm^{-2}) and IrO_2/NF (419±3 mV at 100 mA cm^{-2}) electrocatalysts (Figure S13), making it one of the superior OER catalysts relying on one of the most earth-abundant first-row transition metals. Furthermore, the catalytic activity achieved with Cu_9S_5/NF is much higher than the well-established copper-oxide and/or hydroxides OER catalysts, however, it is comparable to Cu_3N, Cu_3P, and Cu_2Se (Table S4).[10c,17e,18a,19a–c,31] Besides, the catalytic activity of the presented catalysts is also almost comparable to highly-active CoO_x, NiO_x, and Fe doped NiO_x, $Ni_xFe_{1-x}O$ OER catalysts (Table S4).[10a,32]

The OER kinetics of Cu_9S_5/NF, CuO/NF and Cu/NF were investigated by the Tafel slope. The Tafel plots (Figure 3b) of all catalysts were calculated by their corresponding LSV polarization curves. As observed in Figure 3b, the Tafel slope of Cu_9S_5/NF electrode (67±3 mV dec^{-1}) is lower than those of CuO/NF (92±4 mV dec^{-1}), and Cu/NF electrode (146± 3 mV dec^{-1}), indicating a more efficient electron transfer, more favorable electrocatalytic reaction kinetics, and high catalytic activity toward OER for Cu_9S_5/NF. The electron (or charge) transfer capacity was further evaluated by electrochemical impedance spectra (EIS) where Cu_9S_5/NF exhibited the lowest charge-transfer resistance (R_{CT}) than CuO/NF and Cu/NF imply-
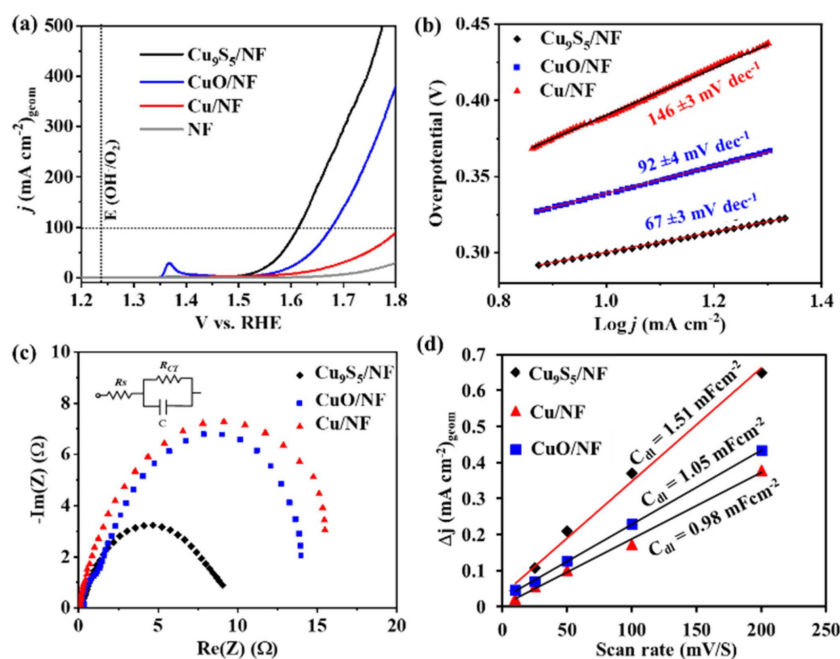

Figure 3. Electrochemical OER activities of Cu_9S_5/NF, CuO/NF, and Cu/NF; (a) OER polarization curves from LSV, (b) Tafel plot, (c) Nyquist plot from EIS analysis (inset: equivalent RC circuit) and (d) double-layer capacitance (C_{dl}) determination from CV scans in a non-Faradaic potential range. (The LSV and Tafel slopes were recorded at a scan rate of 1 mV s^{-1} in 1 M aqueous KOH solution).

ing the smallest electron and charge transfer resistance and thus fast electrode kinetics of Cu_9S_5/NF (Table S5). A better OER activity of Cu_9S_5/NF was achieved due to low R_{CT}, which indicates a spontaneous electron transfer between the electrode surface and electrolyte (Figure 2c).[33] To gain insights into the intrinsic activity of the presented catalysts, we measured the double-layer capacitances (C_{dl}), which could be associated with electrocatalytic active surface areas (ECSAs). A C_{dl} of 1.51 mF cm^{-2} was determined for Cu_9S_5/NF by collecting CVs in a non-faradic region (Figure S14), which is higher than CuO/NF (1.05 mF cm^{-2}) and Cu/NF (0.98 mF cm^{-2}) (Table S6, Figure 3d).[32f,34] From C_{dl}, ECSA was calculated and an ECSA of 0.89 cm^2 was obtained for Cu_9S_5/NF, which is the best among the other copper materials reported herein (Table S6). The ECSA normalized current density obtained for Cu_9S_5 is also higher compared to other copper catalysts used herein, proving a superior intrinsic activity of the Cu_9S_5 catalyst (Figure S14d). Eventually, the long-term durability of Cu_9S_5/NF catalyst was assessed by a chronoamperometry (CA) measurement conducted at 1.55 V (vs. RHE), which maintained a current density above 10 mA cm^{-2} (Figure S15) over 12 h indicating the inherent stability of the catalyst on a longer run. Faradaic efficiency of ~96% for OER was calculated by quantifying the evolved O_2 (gas) during electrolysis at a constant current of 50 mA cm^{-2} using Cu_9S_5/NF as a working electrode (Table S7).

To uncover the role of electrode substrate in electrocatalysis, additionally, Cu_9S_5 was also deposited (via EPD) on fluorine-doped tin oxide (FTO) substrate. Microscopic and analytical studies confirmed the structural integrity of materials deposited on FTO (Figure S16–S18). Under a similar electrochemical OER condition (in 1 M aqueous KOH electrolyte, three-electrode set-up), the LSV of Cu_9S_5/FTO showed an overpotential of 380±3 mV at a current density of 10 mA cm^{-2} while an overpotential of 455±5 and 610±5 mV was required for CuO/FTO and Cu/FTO to achieve the same current density (Figure S19). Interestingly, the presented Cu-based materials deposited on FTO followed a similar trend as that of NF in the reaction of OER.

Recent reports on alkaline OER have suggested that under the electrochemical condition the transition metal-based (non-oxide) materials undergo transformation/corrosion forming an in-situ generated metal-oxide/hydroxide/oxyhydroxide surface overlayer, which is considered as the active species for water oxidation.[10a,d,11,12–14,15e] To understand the structure of active species generated during alkaline OER with Cu_9S_5, we conducted a post electrochemical analysis of the (pre)catalyst using multiple ex-situ microscopic and spectroscopic techniques. The SEM images (Figure S20-21) and successive EDX elemental mapping indicated a considerable amount of oxygen incorporation into the structure, in addition to the initial Cu and S of Cu_9S_5 (Figure 4a-d). High-resolution TEM images of the material, carefully isolated from the electrode surface, indicated the presence of Cu_9S_5 with a thin crystalline overlayer (Figure S22). This thin layer consisted of highly crystalline CuO (JCPDS 72-629) as depicted by the atomic fringes of d(111) planes (Figure 4e). However, atomic fringes at the core displayed d(1010) planes, which belonged to the crystalline core of Cu_9S_5
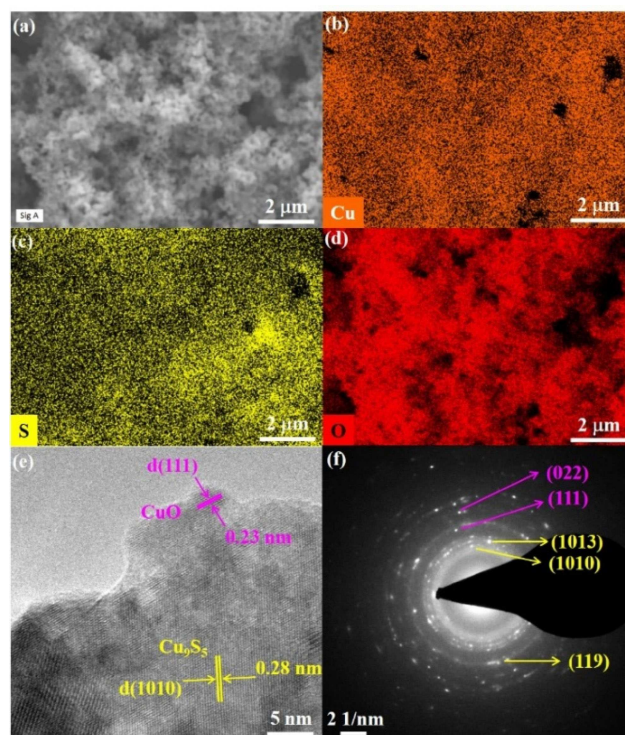

Figure 4. Microscopic characterization of Cu_9S_5 post electrochemical OER. (a) SEM image and (b–d) EDX mapping of elements (Cu, S, and O), (e) high-resolution TEM image after OER with atomic fringes of Cu_9S_5 (JCPDS 47-1748) and CuO (JCPDS 72-629) and (f) SAED pattern exhibiting well-defined diffraction rings Cu_9S_5 and CuO.

(JCPDS 47–1748),[27] and substantiated the formation of CuO@Cu_9S_5 core-shell type structures.[18b,35] The SAED pattern further affirmed this claim with well-defined rings of CuO and Cu_9S_5 (Figure 4f). The elemental composition obtained from the EDX measurement (Figure S23–S24) provided a Cu to S ratio ~1.6:1 and which is due to loss of S from the surface and concomitant incorporation of O into the structure. The surface leaching of S (~20%) in the electrolyte solution was also confirmed by ICP-AES analysis (Table S8).

The surface chemical changes of Cu_9S_5 film post-OER were determined by XPS. The comparison of the binding energy values of Cu 2p, S 2p and spin-orbit splitting of Cu 2p ($2p_{1/2}$–$2p_{3/2}$), of the as-deposited Cu_9S_5 and post-OER films, confirmed a surface structural change under prolonged electrochemical condition. The core level Cu 2p spectra for the post-OER film showed two prominent peaks at 933.3 eV and 953.6 eV for Cu $2p_{3/2}$ and Cu $2p_{1/2}$, respectively, indicating the formation of a substantial amount of Cu^{II} on the surface compared to as-deposited film (Figure 5a).[20b,29] Additionally, the presence of two strong satellite peaks at 942.2 eV and 962.1 eV strongly supports the formation of Cu^{II} on the surface. The S 2p core-level spectra showed a broad and weak signal indicating a negligible amount of sulfur on the surface (Figure 5b). However, the O 1s spectrum after OER displayed a sharp peak at 529.8 eV, suggesting the formation of CuO on the surface to act as an active catalyst along with some amount of surface hydroxides (Figure S25).[31a,36] The results attained from XPS are in good
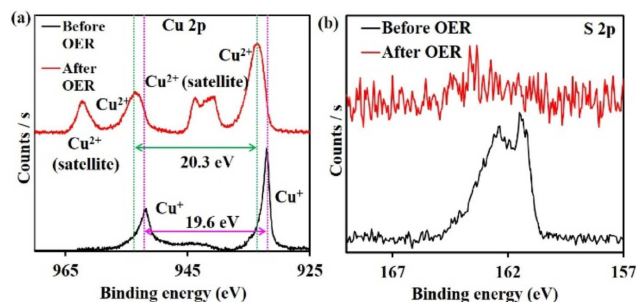
Figure 5. High resolution (a) Cu 2p and (b) S 2p core-level XPS spectra obtained for Cu_9S_5 as-deposited (black curves) and post OER films (red curves). After OER, the Cu 2p indicated the oxidation of Cu to Cu^+ to Cu^{2+} with typical satellite peaks and spin-orbit splitting distance while the negligible amount of S was found on the surface illustrating the concomitant incorporation of O into the structure (Figure S24) forming $CuO@Cu_9S_5$

agreement with the conclusions achieved from SEM, elemental mapping, EDX, ICP-AES, TEM, and SAED.

Overall, the higher catalytic activity of Cu_9S_5 for OER in strongly alkaline conditions could be attributed to the formation of an in-situ crystalline CuO overlayer under applied oxidation potentials that could form $Cu^{III}O(OH)$ species to facilitate O—O bond formation to catalyze the reaction of OER,[10c,20,28,37] while Cu_9S_5 could act as a highly conducting core structure.[20a,31a,37] This observation is in analogy to various Cu-based heterogeneous catalysts applied for OER. Besides, the high ECSA of Cu_9S_5 exposes more active sites for OER while a low charge transfer resistance of Cu_9S_5 signifies better change transport across electrode/electrolyte and vice versa. Finally, the NF was found to be a good choice as an electrode substrate due to its improved conducting nature, increased mass transport and enhancing the dissipation of evolved O_2 gas.

Conclusion

A facile low-temperature molecular precursor route was presented to give the crystalline Cu_9S_5 nanostructure of the *Digenite* mineral. The respective dicopper(I) precursor complex **1** is easily accessible through a simple synthetic protocol using 2-mercapto pyridine as supporting ligand and ${Cu(OTf)_2}$ as Cu source The dinuclear $Cu^I_2S_2$ core in **1** is ideal for building the structurally versatile Cu_9S_5 nano-sized particles, where mixed-valence copper centers are present in three different coordination geometries. The distinct Cu_9S_5 nanostructure, when deposited on electrode substrates, behaves as a potent anode for performing OER in alkaline media displaying considerably low overpotential. A systematic post-OER study revealed that the as-prepared Cu_9S_5 is a pre-catalyst and under applied potentials, forming an in-situ crystalline CuO overlayer that acts as active sites for OER while the superior conductivity of the Cu_9S_5 core promotes a facile charge transport between the catalytic sites to the electrode surface. This facile synthetic method can easily be modified and expanded to the design of high-performance catalysts based on earth-abundant non-noble

metal-based systems for widespread use in various applications, especially for CO_2 reduction, supercapacitors, and lithium-ion batteries.

Experimental Section

General considerations and instrumentation: Synthesis of molecular precursor 1 and Cu_9S_5 manipulations were carried out under dry oxygen-free nitrogen using standard Schlenk techniques. Organic solvents (CH_2Cl_2, diethyl ether) were dried by standard methods and freshly distilled prior to use. Commercially available reagents; 2-mercaptopyridine, $Cu(OTf)_2$ (98%) were purchased from Sigma-Aldrich and used as received. The commercial RuO_2 (99%), IrO_2 (99%), were purchased from Alfa Aesar. NF and FTO, resistivity (8–12 Ω/sq) were obtained from Racemat BV and Sigma Aldrich respectively. The solution NMR spectrum was recorded on Bruker Spectrometers AV 500 with residual solvent signals as internal reference (CD_3CN). The following abbreviations were used to describe peak patterns when appropriate: br = broad singlet, s = singlet, d = doublet, t = triplet, dd = doublet of doublets, m = multiplet. Fourier transform infrared (FTIR) spectra were recorded on a Thermo Fisher Nicolet iS5 IR spectrometer (ATR-Diamond) under inert conditions. High-resolution ESI-MS, APCI-MS were measured on a Thermo Scientific LTQ orbitrap XL. Elemental analyses were recorded in a Thermo FlashEA 1112 Organic elemental analyzer. Related details of crystallographic measurement and the materials characterizations have been discussed in the supporting information.

Preparation of [{(PyHS)₂Cuᴵ(PyHS)}₂](OTf)₂ (1). To a well stirred solution of $Cu(OTf)_2$ (0.500 g, 1.38 mmol) in dichloromethane (10 mL), was added a dichloromethane solution (15 mL) of 2-mercaptopyridinethiol (0.615 g, 5.52 mmol). After stirring the resultant yellow suspension for 8 h under inert atmosphere, solvent was evaporated under vacuum. The residue was washed twice with diethyl ether (2×20 mL), filtered and dried under vacuum. X-ray quality crystals were obtained by keeping concentrated acetonitrile solution of **1** at −20 °C overnight. Yield: 0.990 g (89%). Elemental analysis calculated for $C_{32}H_{30}Cu_2F_6N_6O_6S_8$ (1092.19 g mol^{-1}): C 35.26; H 2.59; N 7.71; S 23.53; found: C 34.9, H 2.7, N 7.6, S 22.9%. IR (ATR, diamond): ν = 3183(br), 3056(m)-2981(m), 1571(s), 1499(s), 1441(s), 1366(s), 1269(m), 1222(s), 1127(s), 1028(s), 750(s), 636(s). ESI-MS (positive ion mode, THF): m/z = 284.96 [Cu(pySH)₂], 395.97 [Cu(pySH)₃]. 1-H NMR (500 MHz, CD_3CN): δ = 12.5 (br, 6H), 7.88 (d, J = 4.6 Hz, 6H), 7.65 (m, 12H), 7.05 (t, J = 5.6 Hz, 6H) ppm. CCDC 1975340 contains the supplementary crystallographic data for this paper. This data is provided free of charge by The Cambridge Crystallographic Data Centre.

Synthesis of Cu_9S_5. To a three-necked round bottom Schlenk flask fitted with a temperature sensor and a condenser, 25 mL olelyl-amine (Fisher Scientific) was added. The solvent was degassed by a 3-cycle freeze-pump method. The whole set-up was degassed using vacuum followed by refilling with nitrogen three times and then the flask was heated to 250 °C. The precursor (0.500 g, 0.5 mmol) was dissolved in 5 mL of dry oleylamine at 30 °C in another flask. The solution was transferred to the three-necked flask at 250 °C by injection under inert conditions. The reaction temperature was maintained at 250 °C for one more hour and then the mixture was allowed to cool down to room temperature. The whole reaction mixture was transferred into a centrifuge tube and centrifuged along with an additional 20 mL ethanol at 9000 rpm to produce a black solid. Washing with ethanol was repeated thrice more to remove any excess ligand and oleylamine. The precipitate was then washed with acetone and dried to store for further use. Yield = 0.055 g. The carbon content was less than 5%.

Synthesis of Cu and CuO.[10c] Solid copper(II) acetate monohydrate (300 mg) was heated to 300 °C with a heating rate of 5 °C min^{-1} and maintained the temperature for 2 hours in an atmosphere of flowing H$_2$ (slow, 2–3 L h^{-1}). The resulting black powder product was washed with water and ethanol (3 × 50 mL) and dried overnight at 60 °C to obtain 100 mg (yield > 90 %) of phase pure Cu. Following a very similar procedure, CuO (yield > 95 %) nanoparticles (NP) were obtained whereas the heating was done in presence of O$_2$ flow

Electrochemical measurements. Electrocatalytic OER was carried out in a standard three-electrode setup consisting of a Hg/HgO as a reference electrode (RE), a Pt wire (0.5 mm diameter × 230 mm length; A-002234, BioLogic) as a counter electrode (CE) and the catalyst-modified working electrode (WE) using an aqueous electrolyte (1 M KOH, Sigma Aldrich). A potentiostat (SP-200, BioLogic Science Instruments) controlled by the EC-Lab v10.20 software package was used for all the electrochemical measurements and further data analyses. Two different substrates NF and FTO were used electrode support. The investigated materials were deposited electrophoretically by a well-established method on both, NF and FTO.[12,14,15e,22,30a] A potential difference of −10 V in a mixture of iodine and acetone on a 1 × 1 cm^2 area was applied. The electric charge on the catalyst in acetone is insufficient for EPD, as minimal amounts of free ions exist in acetone. When iodine is used as the dispersant, it can react with acetone through the keto-enol tautomerization to produce protons as per the following equation.[38]
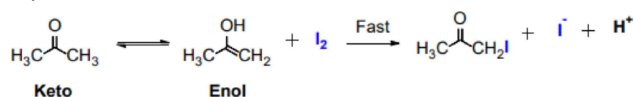
Thus, formed protons are adsorbed on the surface of the suspended particles by making them positively charged. The applied electric field induces the positively charged particles to migrate towards and deposit on the cathode. Typically, 30–40 mg of the catalyst powder was suspended in 10 mL acetone and sonicated for 1 h, then 3 mg of iodine was added and the suspension sonicated for another 3 min. The EPD was conducted at −10 V for 2 min over a 1 × 1 cm^2 surface area of the electrode and thin uniform films were obtained. The sample loading on each NF and FTO was ~0.6 and ~0.5 mg cm^{-2}, respectively. A similar procedure was also followed to deposit other materials (Cu, CuO, RuO$_2$, and IrO$_2$) on NF.

LSV measurements were performed with an applied iR compensation of 85 %, applied before each experiment. The potentials of the reference electrodes in this work were referenced to the reversible hydrogen electrode (RHE) through calibration, and in 1 M aqueous KOH the potential was calculated using the following equations: E(RHE) = E(Hg/HgO) + 0.098 V + (0.059 × pH) V. The potential ranges were 1.2 to 1.8 V vs. RHE for OER. The overpotentials were determined from the resulting polarization curves. The chronoamperometry measurements were performed in 1 M aqueous KOH, and a constant potential 1.55 V vs RHE was applied for 10 h. The polarization curves were plotted as overpotential (η) versus the logarithm of current density (log j) to obtain Tafel plots. The Tafel slope was calculated according to the Tafel equation $\eta = b\log j + a$, where η is the overpotential (V), j is the current density (mA cm^{-2}), and b is the Tafel slope (mV dec^{-1}). Tafel plots were constructed for OER on samples deposited on NF. The region considered for Tafel was on the kinetically controlled region. The double-layer capacitance (C_{dl}) was determined to calculate the active surface area of the materials deposited on the electrode surface.[32f] C_{dl} was calculated from cyclic voltammogram (CV) curves recorded in a potential range with no Faradaic current at different scan rates from 10 to 200 mV s^{-1} (cycled between 0.875 and 0.925 V vs. RHE). The ECSA of the catalysts was calculated using the equation ECSA =

C_{dl}/C_s, where C_s can be defined as the specific capacitance of the material per unit area under identical electrolyte conditions.[39] The specific capacitance (C_s) value of 1.7 mF cm^{-2} based on the literature reported values of NF in 1 M KOH solution is considered to calculate the ECSA. EIS was recorded at 1.51 V vs. RHE for samples deposited on NF to obtain the Nyquist plots. The amplitude of the sinusoidal wave was examined in a frequency range of 100 kHz to 1 mHz. All impedance spectra were fitted using an equivalent RC circuit model. The charge-transfer resistance (R_{CT}) was then obtained from the diameter of the semicircle in the Nyquist plots.[32f]

Acknowledgements

Conflict of Interest

The authors declare no conflict of interest.

Keywords: Copper sulfides · Single-source precursor · *Digenite* · Electrocatalytic OER · Non-noble metal catalysis

[1] a) M. Höök, X. Tang, *Energy Policy* **2013**, *52*, 797–809; b) M. S. Dresselhaus, I. L. Thomas, *Nature* **2001**, *414*, 332–337; c) P. W. Menezes, A. Indra, F. Schuster, M. Schwarze, Gutkin, M. Driess, *ChemPlusChem*, **2016**, *81*, 1068–1074.

[2] a) J. Qi, W. Zhang, R. Cao, *Adv. Energy Mater.* **2018**, *8*, 1701620; b) H. B. Gray, *Nat. Chem.* **2009**, *1*, 7.

[3] a) Y. Wang, H. Suzuki, J. Xie, O. Tomita, D. J. Martin, M. Higashi, D. Kong, R. Abe, J. Tang, *Chem. Rev.* **2018**, *118*, 5201–5241; b) A. J. Nozik, J. Miller, *Chem. Rev.* **2010**, *110*, 6443–6445; c) L. Yuan, C. Han, M.-Q. Yang, Y.-J. Xu, *Int. Rev. Phys. Chem.* **2016**, *35*, 1–36.

[4] a) N.-T. Suen, S.-F. Hung, Q. Quan, N. Zhang, Y.-J. Xu, H. M. Chen, *Chem. Soc. Rev.* **2017**, *46*, 337–365; b) F. Song, L. Bai, A. Moysiadou, S. Lee, C. Hu, L. Liardet, X. Hu, *J. Am. Chem. Soc.* **2018**, *140*, 7748–7759; c) J. Li, R. Güttinger, R. Moré, F. Song, W. Wan, G. R. Patzke, *Chem. Soc. Rev.* **2017**, *46*, 6124–6147; d) T. A. Faunce, W. Lubitz, A. W. Rutherford, D. MacFarlane, G. F. Moore, P. Yang, D. G. Nocera, T. A. Moore, D. H. Gregory, S. Fukuzumi, K. B. Yoon, F. A. Armstrong, M. R. Wasielewski, S. Styring, *Energy Environ. Sci.* **2013**, *6*, 695; e) C. Bozal-Ginesta, J. R. Durrant, *Faraday Discuss.* **2019**, *215*, 439–451; f) J. J. Concepcion, R. L. House, J. M. Papanikolas, T. J. Meyer, *Proc. Natl. Acad. Sci. USA* **2012**, *109*, 15560–15564; g) X. Long, W. Qiu, Z. Wang, Y. Wang, S. Yang, *Mater. Today Chem.* **2019**, *11*, 16–28.

[5] a) D. A. Pantazis, *ACS Catal.* **2018**, *8*, 9477–9507; b) T. J. Meyer, M. V. Sheridan, B. D. Sherman, *Chem. Soc. Rev.* **2017**, *46*, 6148–6169.

[6] a) B. You, Y. Sun, *Acc. Chem. Res.* **2018**, *51*, 1571–1580; b) B. Zhang, L. Sun, *Chem. Soc. Rev.* **2019**, *48*, 2216–2264; c) P. Garrido-Barros, C. Gimbert-Suriñach, R. Matheu, X. Sala, A. Llobet, *Chem. Soc. Rev.* **2017**, *46*, 6088–6098; d) B. Chakraborty, G. Gan-Or, Y. Duan, M. Raula, I. A. Weinstock, *Angew. Chem. Int. Ed.* **2019**, *58*, 6584–6589; e) B. Chakraborty, G. Gan-Or, M. Raula, E. Gadot, I. A. Weinstock, *Nat. Commun.* **2018**, *9*, 4896; f) B. Chakraborty, A. Indra, P. V. Menezes, M. Driess, P. W. Menezes, *Mater. Today Chem.* **2020**, *15*, 100226; g) J. H. Montoya, L. C. Seitz, P. Chakthranont, A. Vojvodic, T. F. Jaramillo, J. K. Nørskov, *Nat. Mater.* **2016**, *16*, 70–81.

[7] a) T. Reier, M. Oezaslan, P. Strasser, *ACS Catal.* **2012**, *2*, 1765–1772; b) Y. Jiao, Y. Zheng, M. Jaroniec, S. Z. Qiao, *Chem. Soc. Rev.* **2015**, *44*, 2060–2086.

[8] a) A. Indra, P. W. Menezes, C. Das, D. Schmeißer, M. Driess, *Chem. Commun.* **2017**, *53*, 8641–8644; b) P. W. Menezes, A. Indra, V. Gutkin, M. Driess, *Chem. Commun.* **2017**, *53*, 8018–8021.

[9] C. Panda, P. W. Menezes, C. Walter, S. Yao, M. E. Miehlich, V. Gutkin, K. Meyer, M. Driess, *Angew. Chem. Int. Ed.* **2017**, *56*, 10506–10510.

[10] a) R. Beltrán-Suito, P. W. Menezes, M. Driess, *J. Mater. Chem. A* **2019**, *7*, 15749–15756; b) S. Yao, V. Forstner, P. W. Menezes, C. Panda, S. Mebs, E. M. Zolnhofer, M. E. Miehlich, T. Szilvási, N. Ashok Kumar, M. Haumann, K. Meyer, H. Grützmacher, M. Driess, *Chem. Sci.* **2018**, *9*, 8590–8597; c) C. Panda, P. W. Menezes, M. Zheng, S. Orthmann, M. Driess, *ACS Energy Lett.* **2019**, *4*, 747–754; d) C. Walter, P. W. Menezes, S. Orthmann, J. Schuch, P. Connor, B. Kaiser, M. Lerch, M. Driess, *Angew. Chem. Int. Ed.* **2018**, *57*, 698–702.

[11] a) P. W. Menezes, C. Panda, S. Garai, C. Walter, A. Guiet, M. Driess, *Angew. Chem. Int. Ed.* **2018**, *57*, 15237–15242; b) P. W. Menezes, C. Walter, J. N. Hausmann, R. Beltran-Suito, C. Schlesiger, S. Praetz, V. Y. Verchenko, A. Shevelkov, M. Driess, *Angew. Chem. Int. Ed.* **2019**, *58*, 16569–16574; *Angew. Chem.* **2019**, *131*, 16722–16727.

[12] P. W. Menezes, C. Panda, C. Walter, M. Schwarze, M. Driess, *Adv. Funct. Mater.* **2019**, *29*, 1808632.

[13] P. W. Menezes, C. Panda, S. Loos, F. Bunschei-Bruns, C. Walter, M. Schwarze, X. Deng, H. Dau, M. Driess, *Energy Environ. Sci.* **2018**, *11*, 1287–1298.

[14] P. W. Menezes, A. Indra, I. Zaharieva, C. Walter, S. Loos, S. Hoffmann, R. Schlögl, H. Dau, M. Driess, *Energy Environ. Sci.* **2019**, *12*, 988–999.

[15] a) I. Roger, M. A. Shipman, M. D. Symes, *Nat. Rev. Chem.* **2017**, *1*, 928; b) B. M. Hunter, H. B. Gray, A. M. Müller, *Chem. Rev.* **2016**, *116*, 14120–14136; c) S. Anantharaj, S. R. Ede, K. Sakthikumar, K. Karthick, S. Mishra, S. Kundu, *ACS Catal.* **2016**, *6*, 8069–8097; d) K. N. Dinh, Q. Liang, C.-F. Du, J. Zhao, A. I. Y. Tok, H. Mao, Q. Yan, *Nano Today* **2019**, *25*, 99–121; e) S. Li, P. Ren, C. Yang, X. Liu, Z. Yin, W. Li, H. Yang, J. Li, X. Wang, Y. Wang, R. Cao, L. Lin, S. Yao, X. Wen, D. Ma, *Sci. Bull.* **2018**, *63*, 1358–1363; f) J. Hu, S. Li, J. Chu, S. Niu, J. Wang, Y. Du, Z. Li, X. Han, P. Xu, *ACS Catal.* **2019**, *9*, 10705–10711.

[16] I. I. Mazin, *Phys. Rev. B* **2012**, *85*, 115133.

[17] a) M. B. Gawande, A. Goswami, F.-X. Felpin, T. Asefa, X. Huang, R. Silva, X. Zou, R. Zboril, R. S. Varma, *Chem. Rev.* **2016**, *116*, 3722–3811; b) A. A. Dubale, A. G. Tamirat, H.-M. Chen, T. A. Berhe, C.-J. Pan, W.-N. Su, B.-J. Hwang, *J. Mater. Chem. A* **2016**, *4*, 2205–2216; c) L. An, L. Huang, P. Zhou, J. Yin, H. Liu, P. Xi, *Adv. Funct. Mater.* **2015**, *25*, 6814–6822; d) Y. Huang, Y. Deng, A. D. Handoko, G. K. L. Goh, B. S. Yeo, *ChemSusChem* **2018**, *11*, 320–326; e) Y. Hong, J. Zhang, F. Huang, J. Zhang, X. Wang, Z. Wu, Z. Lin, J. Yu, *J. Mater. Chem. A* **2015**, *3*, 13913–13919.

[18] a) L. He, D. Zhou, Y. Lin, R. Ge, X. Hou, X. Sun, C. Zheng, *ACS Catal.* **2018**, *8*, 3859–3864; b) Y. Zuo, Y. Liu, J. Li, R. Du, X. Han, T. Zhang, J. Arbiol, N. J. Divins, J. Llorca, N. Guijarro, K. Sivula, A. Cabot, *Chem. Mater.* **2019**, *31*, 7732–7743; c) X. Zhao, L. Liu, Y. Zhang, H. Zhang, Y. Wang, *Nanotechnology* **2017**, *28*, 345402; d) L. An, P. Zhou, J. Yin, H. Liu, F. Chen, H. Liu, Y. Du, P. Xi, *Inorg. Chem.* **2015**, *54*, 3281–3289.

[19] a) H. Liang, W. Shuang, Y. Zhang, S. Chao, H. Han, X. Wang, H. Zhang, L. Yang, *ChemElectroChem* **2018**, *5*, 494–500; b) S. Zhang, Y. Sun, F. Liao, Y. Shen, H. Shi, M. Shao, *Electrochim. Acta* **2018**, *283*, 1695–1701; c) J. Kundu, S. Khilari, K. Bhunia, D. Pradhan, *Catal. Sci. Technol.* **2019**, *9*, 406–417; d) Q. Li, X. Wang, K. Tang, M. Wang, C. Wang, C. Yan, *ACS Nano* **2017**, *11*, 12230–12239.

[20] a) J. Tian, Q. Liu, N. Cheng, A. M. Asiri, X. Sun, *Angew. Chem. Int. Ed.* **2014**, *53*, 9577–9581; b) X. Liu, H. Zheng, Z. Sun, A. Han, P. Du, *ACS Catal.* **2015**, *5*, 1530–1538; c) A. Han, H. Zhang, R. Yuan, H. Ji, P. Du, *ACS Appl. Mater. Interfaces* **2017**, *9*, 2240–2248; d) J. Hao, W. Yang, Z. Huang, C. Zhang, *Adv. Mater. Interfaces* **2016**, *3*, 1600236; e) J. Masud, W. P. R. Liyanage, X. Cao, A. Saxena, M. Nath, *ACS Appl. Energy Mater.* **2018**, *1*, 4075–4083; f) R. Zhou, Y. Huang, J. Zhou, H. Niu, L. Wan, Y. Li, J. Xu, J. Xu, *Dalton Trans.* **2018**, *47*, 16587–16595.

[21] a) C. Panda, P. W. Menezes, M. Driess, *Angew. Chem. Int. Ed.* **2018**, *57*, 11130–11139; *Angew. Chem.* **2018**, *130*, 11298–11308; b) P. W. Menezes, A. Indra, P. Littlewood, C. Göbel, R. Shomaecker, M. Driess, *ChemPlusChem* **2016**, *81*, 370–377.

[22] C. Panda, P. W. Menezes, S. Yao, J. Schmidt, C. Walter, J. N. Hausmann, M. Driess, *J. Am. Chem. Soc.* **2019**, *141*, 13306–13310.

[23] D. Moran, K. Sukcharoenphon, R. Puchta, H. F. Schaefer, P. V. R. Schleyer, C. D. Hoff, *J. Org. Chem.* **2002**, *67*, 9061–9069.

[24] A. V. Chuchuryukin, P. A. Chase, A. M. Mills, M. Lutz, A. L. Spek, G. P. M. van Klink, G. van Koten, *Inorg. Chem.* **2006**, *45*, 2045–2054.

[25] a) P. Halder, D. J. SantaLucia, S. V. Park, J. F. Berry, *Inorg. Chem.* **2019**, *58*, 2270–2274; b) P. Halder, S. Ghorai, S. Banerjee, B. Mondal, A. Rana, *Dalton Trans.* **2017**, *46*, 13739–13744.

[26] a) P. Aslanidis, K. Chrissafis, M. Lalia-Kantouri, *J. Therm. Anal. Calorim.* **2011**, *103*, 797–803; b) S. C. Kokkou, S. Fortier, P. J. Rentzeperis, P. Karagiannidis, *Acta Crystallogr.* **1983**, *C39*, 178–180; c) G. A. Stergioudis, S. C. Kokkou, P. J. Rentzeperis, P. Karagiannidis, *Acta Crystallogr.* **1987**, *C43*, 1685–1688.

[27] G. Donnay, J. D. H. Donnay, G. Kullerud, *Am. Mineral.* **1958**, *43*, 228–242.

[28] a) A. Itzhak, E. Teblum, O. Girshevitz, S. Okashy, Y. Turkulets, L. Burlaka, G. Cohen-Taguri, E. Shawat Avraham, M. Noked, I. Shalish, G. D. Nessim, *Chem. Mater.* **2018**, *30*, 2379–2388; b) W. Bryks, E. Lupi, C. Ngo, A. R. Tao, *J. Am. Chem. Soc.* **2016**, *138*, 13717–13725.

[29] A. B. F. Martinson, S. C. Riha, E. Thimsen, J. W. Elam, M. J. Pellin, *Energy Environ. Sci.* **2013**, *6*, 1868.

[30] a) N. Koura, T. Tsukamoto, HiromasaShoji, T. Hotta, *Jpn. J. Appl. Phys.* **1995**, *34*, 1643–1647; b) P. W. Menezes, A. Indra, A. Bergmann, P. Chernev, C. Walter, H. Dau, P. Strasser, M. Driess, *J. Mater. Chem. A* **2016**, *4*, 10014–10022.

[31] a) J. Du, F. Li, Y. Wang, Y. Zhu, L. Sun, *ChemElectroChem* **2018**, *5*, 2064–2068; b) S. Cui, X. Liu, Z. Sun, P. Du, *ACS Sustainable Chem. Eng.* **2016**, *4*, 2593–2600.

[32] a) J. Qi, W. Zhang, R. Xiang, K. Liu, H.-Y. Wang, M. Chen, Y. Han, R. Cao, *Adv. Sci.* **2015**, *2*, 1500199; b) B. Zhang, C. Li, G. Yang, K. Huang, J. Wu, Z. Li, X. Cao, D. Peng, S. Hao, Y. Huang, *ACS Appl. Mater. Interfaces* **2018**, *10*, 23807–23812; c) K. Fominykh, J. M. Feckl, J. Sicklinger, M. Döblinger, S. Böcklein, J. Ziegler, L. Peter, J. Rathousky, E.-W. Scheidt, T. Bein, D. Fattakhova-Rohlfing, *Adv. Funct. Mater.* **2014**, *24*, 3123–3129; d) G. Wu, W. Chen, X. Zheng, D. He, Y. Luo, X. Wang, J. Yang, Y. Wu, W. Yan, Z. Zhuang, X. Hong, Y. Li, *Nano Energy* **2017**, *38*, 167–174; e) K. Fominykh, P. Chernev, I. Zaharieva, J. Sicklinger, G. Stefanic, M. Döblinger, A. Müller, A. Pokharel, S. Böcklein, C. Scheu, T. Bein, D. Fattakhova-Rohlfing, *ACS Nano* **2015**, *9*, 5180–5188; f) C. C. L. McCrory, S. Jung, J. C. Peters, T. F. Jaramillo, *J. Am. Chem. Soc.* **2013**, *135*, 16977–16987; g) Y. Rao, Y. Wang, H. Ning, P. Li, M. Wu, *ACS Appl. Mater. Interfaces* **2016**, *8*, 33601–33607; h) X. Zhang, H. Xu, X. Li, Y. Li, T. Yang, Y. Liang, *ACS Catal.* **2016**, *6*, 580–588; i) G.-H. Moon, M. Yu, C. K. Chan, H. Tüysüz, *Angew. Chem. Int. Ed.* **2019**, *58*, 3491–3495.

[33] Q. Kang, L. Vernisse, R. C. Remsing, A. C. Thenuwara, S. L. Shumlas, I. G. McKendry, M. L. Klein, E. Borguet, M. J. Zdilla, D. R. Strongin, *J. Am. Chem. Soc.* **2017**, *139*, 1863–1870.

[34] Y. Yoon, B. Yan, Y. Surendranath, *J. Am. Chem. Soc.* **2018**, *140*, 2397–2400.

[35] X. Liu, S. Cui, Z. Sun, Y. Ren, X. Zhang, P. Du, *J. Phys. Chem. C* **2016**, *120*, 831–840.

[36] X. Liu, S. Cui, M. Qian, Z. Sun, P. Du, *Chem. Commun.* **2016**, *52*, 5546–5549.

[37] a) J. Du, Z. Chen, S. Ye, B. J. Wiley, T. J. Meyer, *Angew. Chem. Int. Ed.* **2015**, *54*, 2073–2078; b) C.-C. Hou, W.-F. Fu, Y. Chen, *ChemSusChem* **2016**, *9*, 2069–2073.

[38] Y. Yang, J. Huang, J. Zeng, J. Xiong, J. Zhao, *ACS Appl. Mater. Interfaces* **2017**, *9*, 32801–32811.

[39] a) C. C. L. McCrory, S. Jung, I. M. Ferrer, S. M. Chatman, J. C. Peters, T. F. Jaramillo, *J. Am. Chem. Soc.* **2015**, *137*, 4347–4357; b) S. Anantharaj, S. R. Ede, K. Karthick, S. S. Sankar, K. Sangeetha, P. E. Karthik, S. Kundu, *Energy Environ. Sci.* **2018**, *11*, 744–771.